Quantification of Uncertainty in Brain Tumor Segmentation using Generative Network and Bayesian Active Learning

Rasha Alshehhi[1] and Anood Alshehhi[2]
[1]*New York University Abu Dhabi, U.A.E.*
[2]*Tawam Hospital, Al Ain, U.A.E.*

Keywords: Segmentation, Generative Adversarial Network, Uncertainty, Bayesian Active Learning.

Abstract: Convolutional neural networks have shown great potential in medical segmentation problems, such as brain-tumor segmentation. However, little consideration has been given to generative adversarial networks and uncertainty quantification over the output images. In this paper, we use the generative adversarial network to handle limited labeled images. We also quantify the modeling uncertainty by utilizing Bayesian active learning to reduce untoward outcomes. Bayesian active learning is dependent on selecting uncertain images using acquisition functions to increase accuracy. We introduce supervised acquisition functions based on distance functions between ground-truth and predicted images to quantify segmentation uncertainty. We evaluate the method by comparing it with the state-of-the-art methods based on Dice score, Hausdorff distance and sensitivity. We demonstrate that the proposed method achieves higher or comparable performance to state-of-the-art methods for brain tumor segmentation (on BraTS 2017, BraTS 2018 and BraTS 2019 datasets).

1 INTRODUCTION

Convolutional neural networks (CNNs) have been shown to outperform other segmentation methods in different medical applications (e.g., blood vessels, brain-tumor and lung). Mainly, most previous works focus on maximizing accuracy and less attention has been given to evaluate uncertainty quantification in the network outputs. It is essential to measure uncertainty in medical applications to understand the reliability of the segmentation and identify challenging cases necessitating expert review. On the other hand, neural networks are subject to over-fitting and pixel-based prediction may provide incorrect classification with spurious high confidence.

Many previous works use Bayesian modeling to measure epistemic or aleatoric uncertainty. Epistemic is a result of uncertainty in the model parameters, which can be avoided with given enough data. Aleatoric is a result of noise inherent in the input data (e.g., sensor noise and motion) and unaffected by the amount of available data. There are two categories of aleatoric uncertainty. The first category is homoscedastic uncertainty, which is constant with different inputs. The second category is heteroscedastic uncertainty, which varies with different inputs (Kendall and Gal, 2017).

In this work, we use the generative adversarial model (GAN) (Goodfellow et al., 2014). The GAN performs well with unlabeled samples (unsupervised) or a limited number of labeled samples (semi-supervised). As it is known, the labeled samples are often insufficient in medical applications, difficult to obtain and annotating a large number of samples is time-consuming (Xue et al., 2018). We also utilize Bayesian deep active learning to minimize epistemic uncertainty in medical segmentation. In Bayesian deep active learning, we train a model on a small amount of data (training dataset). We use different acquisition functions that mainly select the most informative samples from a large dataset (pooling dataset). Then, we add selected samples to the previous training dataset and build a new model with the latest training dataset. This process is repeated and the training dataset is increased in size with time (Gal et al., 2017). The primary purpose of active learning is to achieve higher accuracy with fewer training samples. There are different well-known acquisition functions frequently used, such as random (baseline), entropy, margin sampling and least confidence (Wang et al., 2017). These functions usually select informative samples relying on the probability estimation (unsupervised functions). In this work, we introduce new supervised acquisition functions based on distance functions between ground-

Alshehhi, R. and Alshehhi, A.
Quantification of Uncertainty in Brain Tumor Segmentation using Generative Network and Bayesian Active Learning.
DOI: 10.5220/0010341007010709
In *Proceedings of the 16th International Joint Conference on Computer Vision, Imaging and Computer Graphics Theory and Applications (VISIGRAPP 2021) - Volume 4: VISAPP*, pages 701-709
ISBN: 978-989-758-488-6

truth and predicted images: Jaccard, Hausdorff and maximum mean discrepancy (MMD) distances.

This paper is organized as follows. Section 2 shows some previous works used for brain-tumor segmentation: generative adversarial networks and convolutional neural networks with uncertainty functions. Section 3 presents our contributions. Section 4 presents the proposed generative model and Bayesian active learning highlighting new acquisition functions. Experimental results are demonstrated in Section 5. Section 6 summarizes this work.

2 RELATED WORK

In this section, we present the previous works for brain-tumor segmentation that uses generative networks (Section 2.1) and Bayesian deep learning (Section 2.2).

2.1 Generative Adversarial Networks

Some works used generative networks for brain-tumor segmentation. Xue et al. (Xue et al., 2018) was the first authors who proposed a novel end-to-end adversarial neural network, called SegAN. They used a fully-convolutional neural network as a generator and discriminator with a multi-scale L1 loss function to learn spatial detail. Giacomello et al. (Giacomello et al., 2019) extended the previous network SegAN by adding Dice Score to the multi-scale L1 loss function, call SegAN-CAT. However, both works did not estimate the uncertainty of the brain-tumor structure.

2.2 Bayesian Active Learning

As we pointed out previously, uncertainty information is a result of the input data (aleatoric estimation) or model (epistemic estimation). Most previous works focused on epistemic assessment. Gal et al. (Gal et al., 2017) introduced cost-effective selection strategies to Bayesian deep active learning to estimate model uncertainty with high accuracy and less manual annotations. This method achieves promising results in classification problems. However, it is computationally expensive. Kendall and Gal (Kendall and Gal, 2017) combined aleatoric and epistemic uncertainty estimates in Bayesian deep learning for both regression and classification applications. Their methods has ideal performance with noisy data.

There are many studies (Eaton-Rosen et al., 2018; Jungo et al., 2018; Wang et al., 2019a; Wang et al., 2019b) utilized medical uncertainty based either on aleatoric or epistemic estimations, but none of them use Bayesian deep active learning. Wang et al. (Wang et al., 2019a) used a combination of aleatoric and epistemic to estimate uncertainties for whole tumor segmentation. Wang et al. (Wang et al., 2019b) also proposed a cascade of hierarchical CNNs to segment all brain-tumor structures, unlike (Wang et al., 2019a), and used test-time augmentation to obtain not only segmentation outputs but also data-based uncertainty (aleatoric) of all structures of brain-tumor segmentation.

3 CONTRIBUTION

In this work, we use Bayesian deep active learning to estimate the model uncertainty (epistemic) of all brain-tumor structures. Few works address uncertainty in all structures of brain-tumor (e.g., cascade CNNs (Wang et al., 2019b)). We train generative networks with small datasets, use active learning to query more samples using well-known acquisition functions introduced in (Wang et al., 2017) such as entropy, margin sampling, least confidence and random sampling. Usually, active learning is used to query samples with the most informative samples because of limited labeled samples. We introduce three acquisition supervised functions dependent on pixel-to-pixel distances between each brain-tumor structure of both groundtruth and predicted image. We estimate pixel-to-pixel distances and select samples based on the average distance. The distances are Jaccard, Hausdorff and maximum mean discrepancy (MMD) distances.

4 METHOD

This section illustrates the proposed method. It is based on applying Bayesian active learning to the generative adversarial network by selecting uncertain samples and updating the generative model for brain-tumor segmentation. Figure 1 represents an overview of the proposed method.

4.1 Generative Adversarial Network (Figure 1 - I)

Deep generative adversarial network (GAN) (Goodfellow et al., 2014; Isola et al., 2017) is a two-player min-max game. It consists of a generator and a discriminator. The generator (G) captures the data distribution of the real image and produces a synthetic label image. The discriminator (D) differentiates the data distribution of the true label image from the data

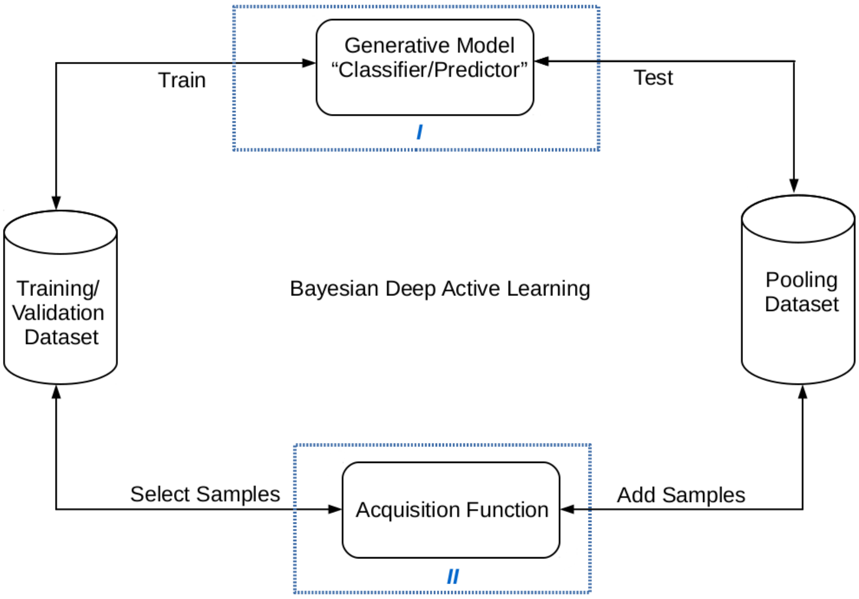

Figure 1: An overview of Bayesian deep active learning. It consists of the following processes: (A) Train the generative model on the training dataset, (B) Test model on a subset of the pooling dataset, (C) Apply unsupervised/ supervised acquisition function on samples and (D) Select samples to add to training dataset and rebuild a new generative model.

distribution of the generator's output label image. The generator and discriminator combat with each other in the training step to minimize an objective function:

$$G^{\star} = \arg\min_{G}\max_{D} \quad L_{cGAN}(G,D) + \lambda L_{l2}(G), \tag{1}$$

where $L_{cGAN}(G,D)$ is a conditional loss of the generative adversarial model and $L_{l2}(G)$ is a mean square error between true label image and generated label image.

$$L_{cGAN}(G,D) = \mathbb{E}_{y\sim\mathbb{P}_r}\left[log(D(x,y)\right] + \mathbb{E}_{G(x)\sim\mathbb{P}_f}\left[log(1-D(x,G(x)))\right], \tag{2}$$

$$L_{l2}(G) = \mathbb{E}_{y\sim\mathbb{P}_r, G(x)\sim\mathbb{P}_f}\left[||y-G(x)||_2\right], \tag{3}$$

where $\mathbb{P}_r$ is the real data distribution and $\mathbb{P}_f$ is the fake data distribution (generated). x and y are input images and true label images. $G(x) = \hat{y}$ is an output label image from the generator. We use uNet with ResNet architecture (He et al., 2016) as a generator. It consists of 8 convolution blocks, which consist of convolution, batch normalization and LeaklyReLU activation. It also consists of 8 deconvolution blocks, consisting of deconvolution, batch normalization and ReLU activation, and skip-connection. It starts with 64 filter kernels of size (4×4). The discriminator network D also has the same architecture. It consists of 8 convolution blocks. Each block consists of convolution, batch normalization and LeaklyReLU activation, starting with 64 kernels of size (4×4). The last layer of convolution is connected with a sigmoid function to generate a distribution map of each class.

4.2 Bayesian Active Learning

The previous network is trained under the Bayesian active learning framework (Gal et al., 2017; Kendall and Gal, 2017). Suppose we use a dataset D_{total} of N samples and C classes:

$$D_{total} = \{(x_0,y_0),(x_1,y_1),(x_2,y_2),...,(x_{N-1},y_{N-1})\} \tag{4}$$

We divide D_{total} into initial training dataset D_{train}, pooling dataset D_{pool} and validation dataset D_{valid}. We start with the initial training dataset D_{train}, validate with validation data D_{valid}. The training dataset incremental grows by selecting samples from D_{pool} based on selection functions called acquisition functions (Figure 1 - II), which we will discuss in detail in this section. The main objective of Bayesian deep active learning is to minimize loss function and improve accuracy.

We fix generative network parameters W. We rank all samples according to the two types of criteria: supervised and unsupervised. The supervised criteria are Jaccard, Hausdorff and MMD distances. The unsupervised criteria are entropy, margin sampling and least confidence (Gal et al., 2017; Wang et al., 2017). After initial training, we test the model M with subset of pooling data D_{pool} for T_{pool} times and select L most uncertain samples from D_{pool} based on selection functions to add to training dataset D_{train}. This process is repeated for T_{train}. The most uncertain ones in the supervised selection approach are with maximum distances between ground-truth y and predicted outputs $\hat{y}$. However, the most uncertain ones in the unsupervised selection approach are with maximum entropy, minimum margin and minimum least confidence.

The supervised selection criteria are based on the maximum pixel to pixel distance between true and predicted images:

- Jaccard distance: it is used as an evaluation metric in segmentation problems. Here we rank samples in D_{pool} in a descending order and select samples of largest distances (more uncertain ones) to add to D_{train} according to:

$$J(y,\hat{y}) = \frac{1}{C}\sum_{c=1}^{C}\frac{y_c \cap \hat{y_c}}{y_c + \hat{y_c} - (y_c \cap \hat{y_c})}, \tag{5}$$

- Hausdorff distance: it is the maximum distance of all pixels from ground-truth image to the corresponding nearest pixel of the predicted segmentation image. Mainly, this distance is used as an evaluation metric or loss function (Isensee et al., 2017; Sauwen et al., 2017). Here we rank samples in D_{pool} in a descending order and select samples of largest distances to add to D_{train} according to:

$$\begin{aligned} H(y,\hat{y}) = \frac{1}{C}\sum_{c=1}^{C}(\frac{1}{N_{y_c}}\sum_{v\in y_c}\min_{w\in\hat{y}_c}\|w-v\|_2 \\ +\frac{1}{N_{\hat{y}_c}}\sum_{w\in\hat{y}_c}\min_{v\in y_c}\|w-v\|_2), \end{aligned} \tag{6}$$

where N_{y_c} and $N_{\hat{y}_c}$ are the number of pixels in ground-truth image y and predicted image $\hat{y}$ of class c.

- Maximum mean discrepancy (MMD): it is usually defined as a distance between two distributions Q_y and $Q_{\hat{y}}$ (Sutherland et al., 2017). Here, we rank samples in D_{pool} in an descending order and select samples of largest distances to add to D_{train} according to:

$$MMD(Q_y,Q_{\hat{y}}) = E_{y\sim Q_y}(y) - E_{\hat{y}\sim Q_{\hat{y}}}(\hat{y}), \tag{7}$$

$$\begin{aligned} MMD(Q_y,Q_{\hat{y}}) = \frac{1}{C}\sum_{c=1}^{C}(\sum_{i\neq j}K(y_i,y_j) \\ -\sum_{i\neq j}K(y_i,\hat{y}_j)+\sum_{i,j}K(\hat{y}_j,\hat{y}_j)), \end{aligned} \tag{8}$$

where $K(y_i,y_j) = \|y_i - y_j\|_2$; i and j are pixels either on ground-truth image y or predicted image $\hat{y}$. $K(y_i,y_j)$ and $K(\hat{y}_i,\hat{y}_j)$ show within distribution similarity; however, $K(y_i,\hat{y}_j)$ show cross distribution similarity.

We also use in conjunction with previous methods, unsupervised criteria from (Gal et al., 2017; Wang et al., 2017). The selection is based on probability of pixel x belonging to the class c $P(y=c|x;W)$; where c is the index of class:

- Entropy: we rank samples in a descending order. The higher entropy sample is more uncertain one:

$$EN(y) = -\sum_{c=1}^{C}P(y=c|x;W)\times logP(y=c|x;W), \tag{9}$$

- Margin sampling: we rank samples based on the first (a) and second (b) most probability class predicted by the model. The smaller margin means more uncertain.

$$MS(y) = P(y_i=c_a|x;W) - P(y_i=c_b|x;W), \tag{10}$$

- Least confidence: we rank samples in an ascending order. The lower least confidence is the more uncertain one.

$$LC(y) = max_cP(y=c|x;W), \tag{11}$$

5 EXPERIMENTAL PERFORMANCE

In the previous section, we present the proposed method highlighting acquisition functions, which will measure the generative network's uncertainty. In this section, we illustrate the performance of the generative networks with various query functions. Section 5.1 and Section 5.2 present used data, setting and evaluation metrics. Section 5.3 shows some results of the proposed method compared to other methods.

5.1 Data

We use datasets of medical image computing and computer-assisted intervention (MICCAI) of multi-modal brain-tumor segmentation (BraTS) Challenge 2017, 2018 and 2019 (Bakas et al., 2017; Menze et al., 2015). The BraTS 2017 and BraTS 2018 share the same dataset. It comprises 285 multi-institutional pre-operative multi-modal magnetic resonance imaging (MRI) scans glioblastoma (GBM/HGG) (210 scans) and lower-grade glioma (LGG) (75 scans). The BraTS 2019 consists of a total of 335 MRI volumes (259 HGG and 76 LGG). The BraTS data is available in (https://www.med.upenn.edu/sbia/) and (https://www.med.upenn.edu/cbica/). Each multi-modal scan consists of native (T1) and post-contrast T1-weighted (T1Gd), T2-weighted (T2) and T2 Fluid Attenuated

Inversion Recovery (FLAIR) volumes. Each volume of size 240×240 consists of 155 slices. The ground-truth volume $240 \times 240 \times 155$ of each scan comprises of peritumoral edema (ED — label 2), necrotic and non-enhancing tumor core (NCR/NET — label 1) and GD-enhancing tumor (ET — label 4). The whole tumor (WT) includes ED, NCR/NET and ET, core tumor (TC) includes NCR/NET and ET and enhanced tumor (ET) includes only ET.

5.2 Experimental Setup and Metrics

The dataset of MICCAI BraTS is divided into four subsets: initial training D_{train} (20 samples), validation D_{valid} (30 samples), pooling D_{pool} (190 samples for BraTS 2017-2018 and 240 for BraTS 2019) and testing samples D_{test} (45 samples). The training process is run for 5 times (number of experiments, $N_e = 5$); at each experiment (i_e), the 3D networks are trained with initial training set D_{train} and evaluate with validation set D_{valid}. At each experiment i_e, the networks are run for 10 times (number of queries, $N_q = 10$). At each query (i_q), the networks are evaluated with a pooling set for 10 times (Monte Carlo (MC) dropout iterations, $N_d = 10$). Based on the results of acquisition functions in each query (i_q), 10 samples are retrieved from pooling set and the networks are retrained using previous initial training set D_{train} and subset of pooling data D_{pool}. We assess the uncertainty in prediction outputs by applying acquisition functions dependent on probabilities of predicted images (entropy, margin sampling or least confidence) or distance between ground-truth and predicted images (jaccard, Hausdorff or MMD).

We compare the proposed method with two convolutional networks (Isensee et al., 2017; Myronenko, 2018). We use the same training procedures used in both works with the same loss functions: Dice coefficient, L2 and KL. We also compare with state-of-the-art networks (Jungo et al., 2018; Wang et al., 2019b; Giacomello et al., 2019; Xue et al., 2018; Mazumdar, 2020) and use the same training procedures with multi-scale L1 loss and Dice coefficient. We use Disc score, Hausdorff score and true positive rate (TPR)/sensitivity to evaluate enhancing tumor (ET), necrotic and non-enhancing tumor core (NCR/NET) and edema (ED) structures. We run all experiments on Nvidia Tesla V100 GPUs-32 GB with Keras 2 of Tensorflow 1.4.

5.3 Results

In this section, we compare the performance of the proposed method with common convolutional networks on BraTS 2017 on BraTS 2018 datasets in Section 5.3.1 and Section 5.3.2 and with state-of-the-art methods on BraTS 2019 in Section 5.3.3.

5.3.1 Comparison the Proposed Method with Isensee's Network on BraTS 2017 Dataset

F. Isensee (Isensee et al., 2017) uses uNet architecture and Dice coefficient as a loss function to cope with class imbalance. Data augmentation is used to avoid over-fitting. This work was one of the leading methods in BraTS 2015 and BraTS 2017.

In Figure 2, we compare the results of applying Isensee's network (Isensee et al., 2017) and generative networks with Bayesian active learning utilizing previous acquisition functions. The predicted images, based on unsupervised functions random, entropy, margin sampling and least confidence, show more uncertainty and overlap sub-regions between ED and NCR/NET borders and many regions that are potentially segmented incorrectly 2(c)-2(f). The predicted image based on Jaccard distance 2(g) also shows relatively higher uncertainty between NCR/NET and ED than the interior structure (ET). However, predicated images based on Hausdorff and MMD distances 2(h)-2(i) have lower uncertainty, in particularity where other uncertainty maps 2(c)-2(g) mismatches with ground-truth map 2(a). The uncertainty Hausdorff and MMD maps identify the previous boundaries with misclassified some NCR/NET pixels, similar to Isensee's model 2(b). The prediction uncertainty maps, either supervised or unsupervised, reflect a lack of confidence around boundaries between different classes, which is changed by increasing the number of experiments, number of queries, number of MC dropout iterations or number of training samples in addition to the type of acquisition function. However, it is computationally expensive, requiring more time and memory usage.

In Table 1, we compare the results obtained by previous models on BraTS 2017 dataset. The Dice score, Hausdorff distance and sensitivity of both supervised and unsupervised methods are comparable. However, it is remarkable that the networks that acquire samples with Hausdorff distance and then with MMD distances show low uncertainty and have the best performance (higher Disc score, lower Hausdorff distance and higher sensitivity). On the other hand, uncertainty entropy maps have higher Dice scores and sensitivity (lower uncertainty) than random, margin and least-confidence maps.

5.3.2 Comparison the Proposed Method with Myronenko's Network on BraTS 2018 Dataset

A. Myronenko (Myronenko, 2018) uses 3D variational encoder-decoder for automated segmentation of brain-

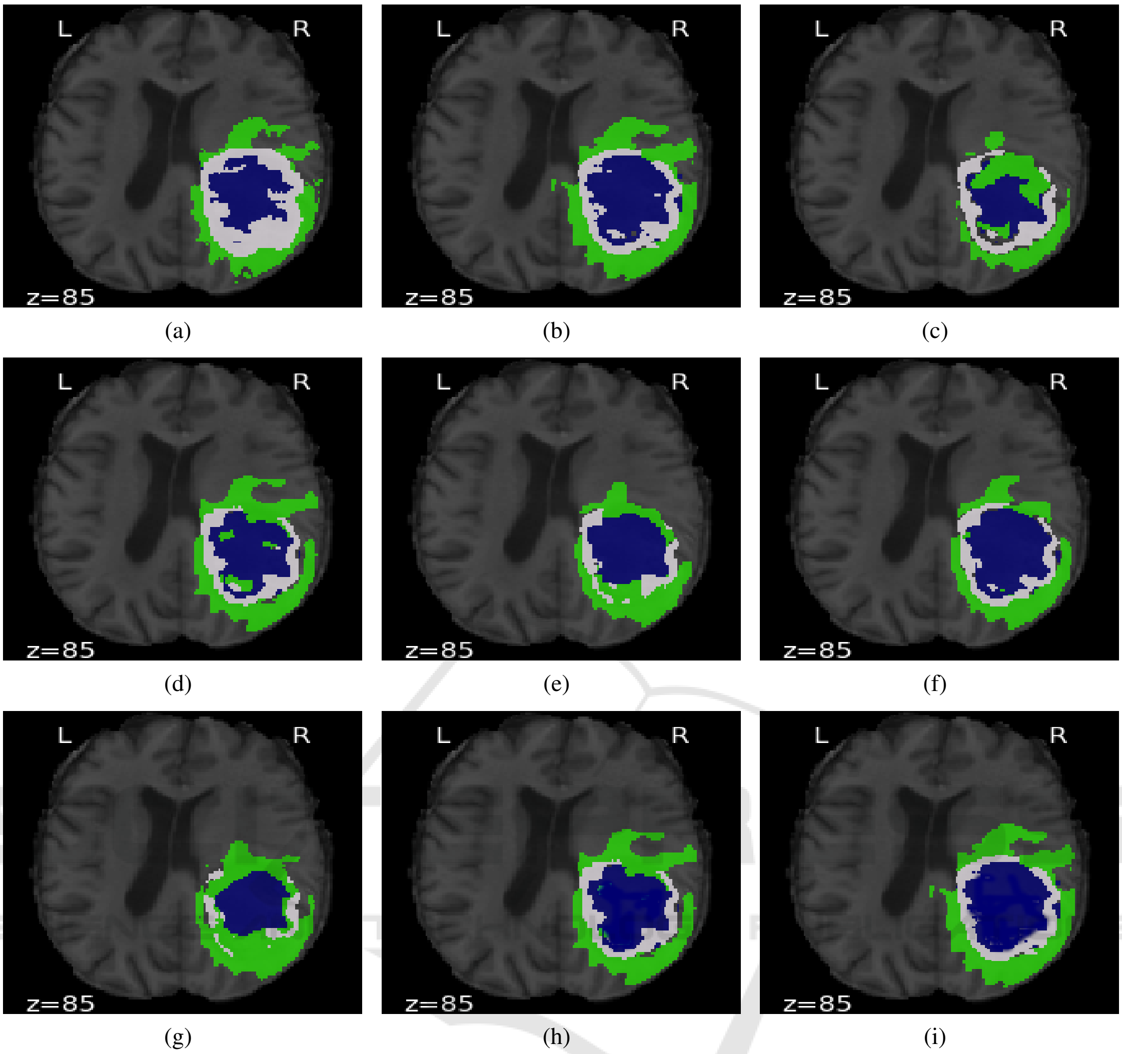

(a) (b) (c)

(d) (e) (f)

(g) (h) (i)

Figure 2: Comparison between predicted images obtained from Isensee's network and generative network using acquisition functions: (a) Ground-truth, (b) Isensee (Isensee et al., 2017), (c) Random sampling, (d) Entropy, (e) Margin sampling, (f) Least confidence, (g) Jaccard, (h) Hausdorff and (i) MMD. Edema (ED) is shown in green, enhancing tumor (ET) in blue and necrotic and non-enhancing tumor (NCR/NET) in white. z is the index of slice.

Table 1: Comparison between Isensee's network and generative network with acquisition functions based on Dice, Hausdorff and sensitivity metrics (mean±std). RS: random sampling, EN: entropy, MS: margin sampling, LC: least confidence, JD: Jaccard distance, HD: Hausdorff distance and MMD: MMD distance. WT, TC and ET denote the whole tumor, tumor core and enhancing tumor.

Method	Dice			Hausdorff			Sensitivity		
	WT	TC	ET	WT	TC	ET	WT	TC	ET
Isensee	0.86 ± 0.09	0.59 ± 0.12	0.74 ± 0.12	5.51 ± 2.19	7.52 ± 2.18	2.42 ± 1.38	0.89 ± 0.09	0.62 ± 0.23	0.79 ± 0.19
RS	0.79 ± 0.18	0.52 ± 0.15	0.63 ± 0.15	7.68 ± 2.11	9.69 ± 2.16	7.22 ± 2.12	0.86 ± 0.19	0.59 ± 0.25	0.77 ± 0.23
EN	0.84 ± 0.14	0.53 ± 0.14	0.66 ± 0.12	6.10 ± 2.16	6.49 ± 2.15	6.28 ± 2.15	0.88 ± 0.16	0.59 ± 0.25	0.78 ± 0.23
MS	0.81 ± 0.17	0.80 ± 0.17	0.62 ± 0.11	7.49 ± 2.16	7.71 ± 2.04	8.47 ± 1.24	0.85 ± 0.18	0.58 ± 0.20	0.74 ± 0.20
LC	0.83 ± 0.16	0.54 ± 0.18	0.67 ± 0.18	7.26 ± 2.39	6.68 ± 1.19	5.76 ± 1.84	0.88 ± 0.14	0.59 ± 0.12	0.79 ± 0.13
JD	0.80 ± 0.17	0.56 ± 0.19	0.67 ± 0.13	5.00 ± 2.15	6.02 ± 2.18	4.01 ± 2.85	0.86 ± 0.19	0.61 ± 0.25	0.77 ± 0.11
HD	0.88 ± 0.18	0.62 ± 0.19	0.75 ± 0.12	5.11 ± 2.17	6.11 ± 2.18	4.03 ± 1.15	0.91 ± 0.15	0.64 ± 0.15	0.80 ± 0.14
MMD	0.87 ± 0.17	0.59 ± 0.19	0.73 ± 0.12	5.01 ± 2.17	5.89 ± 2.18	4.83 ± 1.88	0.90 ± 0.19	0.64 ± 0.15	0.79 ± 0.11

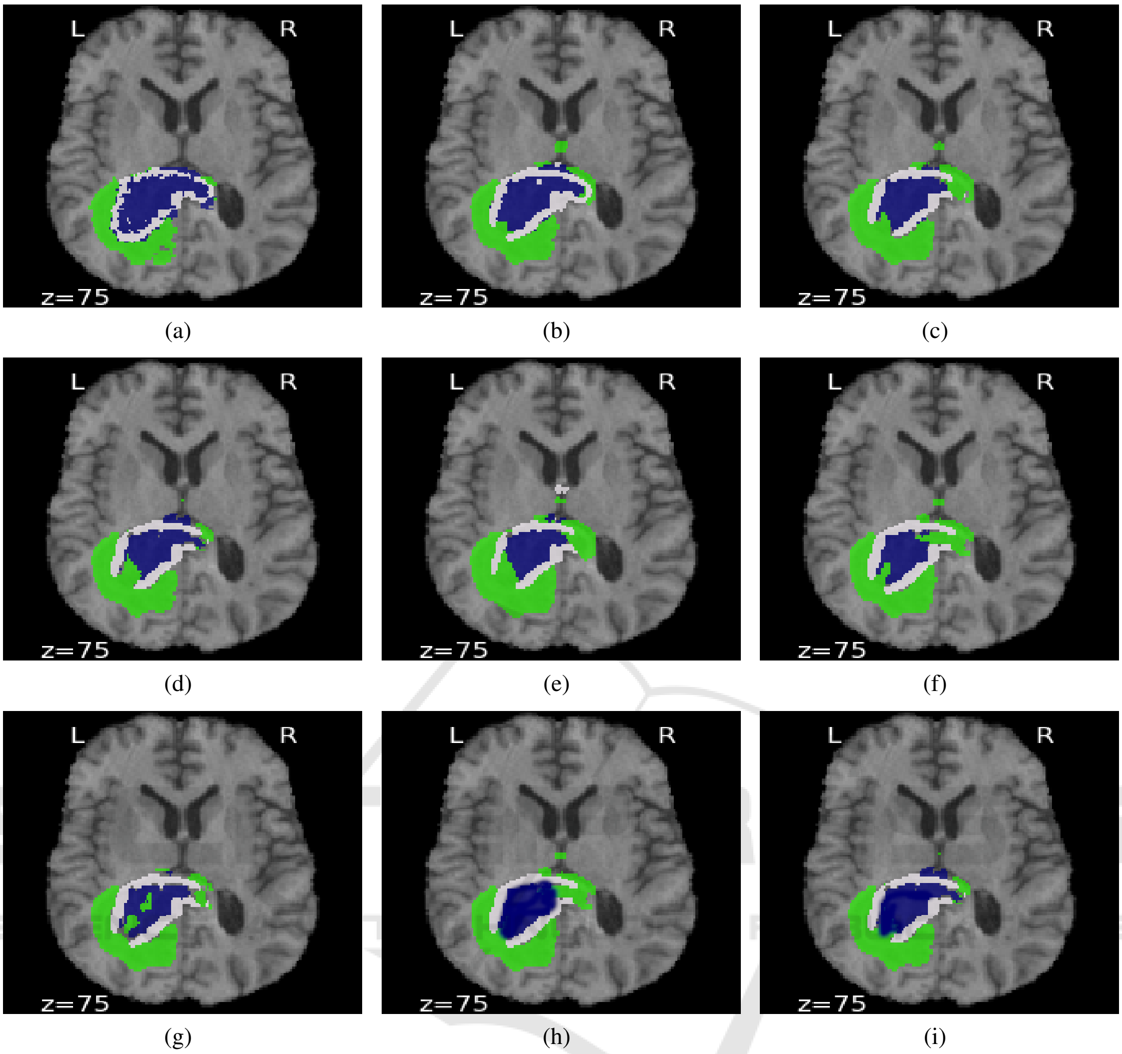

(a) (b) (c) (d) (e) (f) (g) (h) (i)

Figure 3: Comparison between predicted images obtained from using Myronenko's network (Myronenko, 2018) and generative network with acquisition functions: (a) Ground-Truth, (b) Myronenko, (c) Random sampling, (d) Entropy, (e) Margin sampling, (f) Least confidence, (g) Jaccard, (h) Hausdorff and (i) MMD. Edema (ED) is shown in green, enhancing tumor (ET) in blue and necrotic and non-enhancing tumor (NCR/NET) in white. z is the index of slice.

tumor due to limited training data. The author reconstructs the input image to regularize the decoder and impose additional constraints on its layers. This work ranked as 1st place in the BraTS 2018 challenge.

Figure 3 shows an example from the BraTS 2018 dataset. In figure 3(g), the result of the 3D generative network using Jaccard distance contains some false positives in ED, NCR/NET and ET regions associated with higher uncertainties. In contrast, the results of 3D generative networks using Hausdorff and MMD distances 3(h)-3(i) are smoother, particularly in ET regions; reflecting lower uncertainty in hierarchical structures from larger to smaller. On the other hand, unsupervised functions 3(c)-3(f) show uncertainty in larger structure (misclassified ED pixels).

We also show obtained results from all unsupervised and supervised methods on BraTS 2018 in Table 2. Although Myronenko's model (Myronenko, 2018) shows a high Dice score, small Hausdorff distance and high true positive rate, the MMD and then HD maps show the lowest uncertainty, respectively; showing a good correlation between uncertainty and MMD distance or Hausdorff maps. On the other hand, the network based on entropy has lower uncertainty outputs than other ground truth independent maps: MS and LC.

Table 2: Comparison between Myronenko's network and generative network with acquisition functions based on Dice, Hausdorff and sensitivity metrics (mean±std). RS: random sampling, EN: entropy, MS: margin sampling, LC: least confidence, JD: Jaccard distance, HD: Hausdorff distance and MMD: MMD distance. WT, TC and ET denote the whole tumor, tumor core and enhancing tumor.

Method	Dice			Hausdorff			Sensitivity		
	WT	TC	ET	WT	TC	ET	WT	TC	ET
Myronenko	0.90 ± 0.19	0.86 ± 0.12	0.81 ± 0.11	5.51 ± 1.90	6.85 ± 1.11	3.92 ± 1.38	0.90 ± 0.11	0.72 ± 0.13	0.80 ± 0.11
RS	0.80 ± 0.18	0.70 ± 0.18	0.60 ± 0.15	8.18 ± 1.99	9.69 ± 1.96	6.22 ± 1.72	0.79 ± 0.11	0.63 ± 0.14	0.71 ± 0.13
EN	0.85 ± 0.13	0.73 ± 0.18	0.72 ± 0.12	6.10 ± 1.76	6.54 ± 1.95	4.28 ± 1.45	0.82 ± 0.16	0.60 ± 0.15	0.72 ± 0.12
MS	0.81 ± 0.16	0.77 ± 0.11	0.71 ± 0.11	7.49 ± 1.76	8.71 ± 1.04	7.41 ± 1.42	0.80 ± 0.20	0.61 ± 0.16	0.70 ± 0.17
LC	0.84 ± 0.16	0.70 ± 0.11	0.67 ± 0.12	7.21 ± 1.39	8.05 ± 1.99	5.55 ± 1.84	0.78 ± 0.17	0.62 ± 0.14	0.69 ± 0.11
JD	0.82 ± 0.18	0.74 ± 0.19	0.70 ± 0.14	7.56 ± 1.67	7.69 ± 1.98	5.94 ± 1.87	0.85 ± 0.19	0.61 ± 0.15	0.71 ± 0.11
HD	0.91 ± 0.11	0.87 ± 0.15	0.81 ± 0.20	5.56 ± 1.76	5.89 ± 1.95	3.88 ± 1.25	0.90 ± 0.12	0.71 ± 0.15	0.81 ± 0.17
MMD	0.92 ± 0.12	0.88 ± 0.11	0.82 ± 0.21	5.20 ± 1.76	5.01 ± 1.95	3.48 ± 1.15	0.93 ± 0.16	0.73 ± 0.12	0.82 ± 0.12

Table 3: Comparison between different CNN architectures based on Dice score and Hausdorff distance (mean±std). EN and HD are Entropy and Hausdorff distance. WT, TC and ET denote the whole tumor, tumor core and enhancing tumor.

Method	Dice			Hausdorff		
	WT	TC	ET	WT	TC	ET
CNN+Uncertainty (Jungo et al., 2018)	0.89 ± 0.09	0.78 ± 0.12	0.74 ± 0.28	5.41 ± 1.71	7.48 ± 1.94	5.38 ± 1.07
Cascaded CNN+Uncertainty (Wang et al., 2019b)	0.90 ± 0.05	0.83 ± 0.13	0.78 ± 0.18	6.97 ± 2.56	6.78 ± 2.26	4.28 ± 1.07
Fully Residual CNNs (Mazumdar, 2020)	0.89 ± 0.12	0.82 ± 0.11	0.78 ± 0.12	6.38 ± 1.12	5.91 ± 1.21	4.43 ± 1.12
SegAN (Xue et al., 2018)	0.84 ± 0.12	0.61 ± 0.20	0.64 ± 0.28	7.57 ± 2.33	6.63 ± 1.11	5.60 ± 1.22
SegAN-CAT (Giacomello et al., 2019)	0.86 ± 0.14	0.63 ± 0.20	0.68 ± 0.28	7.79 ± 1.33	6.65 ± 1.11	5.66 ± 1.22
Unsupervised EN	0.87 ± 0.32	0.65 ± 0.12	0.68 ± 0.11	6.51 ± 1.21	6.19 ± 1.15	5.69 ± 1.21
Supervised HD	0.89 ± 0.11	0.82 ± 0.11	0.77 ± 0.17	5.01 ± 1.21	5.21 ± 1.15	4.11 ± 1.15

5.3.3 Comparison the Proposed Method with State-of-the-Art Methods on BraTS 2019 Dataset

In Table 3, we compare the proposed method after utilizing unsupervised EN and supervised HD with the state-of-the-art methods that employ uncertainly with 3D CNN (Jungo et al., 2018), 2.5D CNN (Wang et al., 2019b), 2D CNN fully residual CNNs (Mazumdar, 2020), generative adversarial networks (Xue et al., 2018; Giacomello et al., 2019) on the BraTS 2019 dataset. Both methods that utilize MC dropout have high Disc scores, as it is expectant that uncertainly with MC Dropout improves segmentation performance (Gal et al., 2017; Kendall and Gal, 2017). I. Mazumdar (Mazumdar, 2020) achieves higher scores compared to uncertainly and generative methods while it uses 2D fully CNNs with less time and memory usage. Giacomello et al. (Giacomello et al., 2019) improved the SegGAN proposed by (Xue et al., 2018) by adding dice loss to multi-scale L1 loss. Therefore, it has better performance in detecting overlap areas between various sub-regions. Applying generative models with Bayesian active learning, either supervised or unsupervised, increases the accuracy of all structures. As expected, querying samples based on the distance between ground-truth and predicted samples outperforms querying samples based on informative samples. It is also worth mentioning, generative models with supervised HD have the lowest mean and lowest spread of Hausdorff distance compared to all previous methods. This proves that generative models efficiently work with a limited amount of samples, particularly when querying labeled samples.

6 CONCLUSION

Most existing brain-tumor segmentation methods use convolutional networks and do not estimate uncertainty using Bayesian active learning because it is computationally expensive. On the other hand, few methods use generative networks and also do not use uncertainty metrics. In this paper, we use the generative network and explore the uncertainty in all brain-tumor structures. We propose three supervised functions to query uncertain samples based on the distance between ground-truth and predicted outputs: Jaccard, Hausdorff and MMD. We also use, in conjunction with supervised functions, unsupervised criteria: entropy, margin sampling, least-confidence and random sampling. We compare the performance of generative networks using various acquisition functions with two common convolutional networks and state-of-the-art networks used for brain-tumor segmentation. We found that generative networks with supervised query functions have better or comparable performance to generative networks with unsupervised query functions. Besides, the proposed method outperforms previous state-of-the-art networks. There are many false-positive cases by applying all methods, particularly around borders between ET and NCT/NET or NCT/NET and ED because all classes do not have the apparent shape or have indefinite boundaries. The proposed method is a promising direction for studying the feasibility of generative networks with Bayesian active learning to measure uncertainty in segmentation applications. In the future, we aim to investigate the potential of the proposed method to estimate uncertainty in other applications.

REFERENCES

Bakas, S., Akbari, H., Sotiras, A., Bilello, M., Rozycki, M., Kirby, J. S., Freymann, J. B., Farahani, K., and Davatzikos, C. (2017). Advancing the cancer genome atlas glioma MRI collections with expert segmentation labels and radiomic features. *Scientific Data*.

Eaton-Rosen, Z., Bragman, F., Bisdas, S., Ourselin, S., and Cardoso, M. J. (2018). Towards safe deep learning: accurately quantifying biomarker uncertainty in neural network predictions. In *Medical Image Computing and Computer Assisted Intervention*.

Gal, Y., Islam, R., and Ghahramani, Z. (2017). Deep bayesian active learning with image data. In *Proceedings of the 34th International Conference on Machine Learning*, volume 70, pages 1183–1192.

Giacomello, E., Loiacono, D., and Mainardi, L. (2019). Brain MRI tumor segmentation with adversarial networks. *arXiv:1910.02717*.

Goodfellow, I., Pouget-Abadie, J., Mirza, M., Xu, B., Warde-Farley, D., Ozair, S., Courville, A., and Bengio, Y. (2014). Generative adversarial nets. In *Advances in Neural Information Processing Systems 27*, pages 2672–2680.

He, K., Zhang, X., Ren, S., and Sun, J. (2016). Deep residual learning for image recognition. In *IEEE Conference on Computer Vision and Pattern Recognition*, pages 770–778.

Isensee, F., Kickingereder, P., Wick, W., Bendszus, M., and Maier-Hein, K. H. (2017). Brain tumor segmentation and radiomics survival prediction: contribution to the BRATS 2017 challenge. In *3rd International Workshop, BrainLes, Held in Conjunction with Medical Image Computing for Computer Assisted Intervention*, volume 10670, page 287–297.

Isola, P., Zhu, J., Zhou, T., and Efros, A. A. (2017). Image-to-image translation with conditional adversarial networks. In *IEEE Conference on Computer Vision and Pattern Recognition*, pages 5967–5976.

Jungo, A., Meier, R., Ermis, E., Herrmann, E., and Reyes, M. (2018). Uncertainty-driven sanity check: application to postoperative brain tumor cavity segmentation. In *1st Conference on Medical Imaging with Deep Learning*.

Kendall, A. and Gal, Y. (2017). What uncertainties do we need in bayesian deep learning for computer vision? In *Advances in Neural Information Processing Systems 30*, pages 5574–5584.

Mazumdar, I. (2020). Automated brain tumour segmentation using deep fully residual convolutional neural networks. *arXiv:1908.04250*.

Menze, B., Jakab, A., Bauer, S., Kalpathy-Cramer, J., Farahaniy, K., Kirby, J., Burren, Y., Porz, N., Slotboomy, J., Wiest, R., Lancziy, L., Gerstnery, E., Webery, M.-A., Arbel, T., Avants, B., Ayache, N., Buendia, P., Collins, L., Cordier, N., and Van Leemput, K. (2015). The multimodal brain tumor image segmentation benchmark (BRATS). *IEEE Transactions on Medical Imaging*, 34(10):1993–2024.

Myronenko, A. (2018). 3D MRI brain tumor segmentation using autoencoder regularization. In *4rd International Workshop on Brainlesion, BrainLes, Held in Conjunction with Medical Image Computing for Computer Assisted Intervention*, volume 11384, pages 311–320.

Sauwen, N., Acou, M., Sima, D. M., Veraart, J., Maes, F., Himmelreich, U., Achten, E., and Huffel, S. V. (2017). Semi-automated brain tumor segmentation on multi-parametric MRI using regularized non-negative matrix factorization. *BMC Medical Imaging*.

Sutherland, D. J., Tung, H., Strathmann, H., De, S., Ramdas, A., Smola, A. J., and Gretton, A. (2017). Generative models and model criticism via optimized maximum mean discrepancy. In *5th International Conference on Learning Representations*.

Wang, G., Li, W., Aertsen, M., Deprest, J., Ourselin, S., and Vercauteren, T. (2019a). Aleatoric uncertainty estimation with test-time augmentation for medical image segmentation with convolutional neural networks. *Neurocomputing*, 338:34 – 45.

Wang, G., Li, W., Ourselin, S., and Vercauteren, T. (2019b). Automatic brain tumor segmentation based on cascaded convolutional neural networks with uncertainty estimation. *Frontiers in Computational Neuroscience*, 13(56).

Wang, K., Zhang, D., Li, Y., Zhang, R., and Lin, L. (2017). Cost-effective active learning for deep image classification. *IEEE Transactions on Circuits and Systems for Video Technology*, 27(12):2591–2600.

Xue, Y., Xu, T., Zhang, H., Long, L. R., and Huang, X. (2018). SegAN: adversarial network with multi-scale l1 loss for medical image segmentation. *Neuroinformatics*, 16:383–392.